



ELSEVIER

Contents lists available at ScienceDirect

## Spectrochimica Acta Part B: Atomic Spectroscopy

journal homepage: www.elsevier.com



## Laser induced plasmas at different nebulization conditions: Spatio-temporal distribution of emission signals and excitation temperatures

C. Méndez-López<sup>a</sup>, R. Álvarez-García<sup>a,1</sup>, C. Alvarez-Llamas<sup>b</sup>, L.J. Fernández-Menéndez<sup>a</sup>, C. González-Gago<sup>a</sup>, J. Pisonero<sup>a</sup>, N. Bordel<sup>a,\*</sup>

<sup>a</sup> University of Oviedo, Department of Physics, Federico García Lorca 18, 33007 Oviedo, Spain

<sup>b</sup> University of Málaga, Department of Analytical Chemistry, UMA LASERLAB, Jiménez Fraud 4, 29010 Malaga, Spain

### ARTICLE INFO

#### Keywords:

Laser induced breakdown spectroscopy (LIBS)  
Nebulization  
Excitation temperatures  
Plasma plume  
Molecular and atomic emission signals  
Spatio-temporal distribution

### ABSTRACT

CaF emission measurements are currently employed for indirect determination of fluorine concentration in solid samples using LIBS. This approach provides more sensitivity and improved limits of detection in comparison to the use of F atomic emission lines in the IR region, for quantitative purposes. Moreover, in Ca-free samples, the simultaneous nebulization of a Ca-containing solution during LIBS analysis was successfully proposed as a method to obtain the CaF emission, and indirectly determine the F concentration. Nevertheless, further insights are still required to understand the interaction of the laser-induced plasma with the nebulized solution. Therefore, in this work, the general effects of different nebulization conditions on a laser induced plasma are investigated in terms of variations in the plasma plume shapes, emission intensities and excitation temperatures. In particular, four different conditions are evaluated using Cu matrix as a model sample (i.e. non-nebulized sample, Ar nebulization, water nebulization and Ca-containing solution nebulization). Significant changes were shown under the Ca-solution nebulization, including a modification of the intensity decays of the Cu lines, lower average Cu excitation temperatures independently of the temporal window investigated, increased ablation rates, a huge asymmetry of the excited species in the plasma plume, and a partial detachment of the plume.

### 1. Introduction

Laser-Induced Breakdown Spectroscopy (LIBS) is a versatile analytical technique, in which a pulsed laser is focused on a sample's surface. Given that a threshold fluency is surpassed, this interaction produces the ablation of material from the sample and induces a plasma. The different processes taking place within this plasma (atomization, ionization, excitation, recombination...) are translated into characteristic radiation emission from the present neutral, ionized and molecular excited species, which ultimately provides chemical and physical information from the plasma. In principle, LIBS provides direct and simultaneous elemental information from all elements in the periodic table.

Additionally, molecular information can also be obtained in LIBS analysis, resulting of great utility in some applications, for instance: C<sub>2</sub> or CN molecular bands were successfully studied for the discrimination of explosives [1,2,3] and the identification of bacteria [4] or pollen [5]; detection of molecular emission bands combined with multivari-

ate data treatment procedures was suitable assayed for quantification of organic material [6]; isotopic analysis was demonstrated based on the wavelength shift of the emission bands from diatomic molecules differing in an isotope [7,8]; and molecular emission detection resulted beneficial for the determination of halogens, which present very low elemental emission in the spectral range covered by conventional spectrographs (200–1000 nm). For chlorine and fluorine determination, it was reported that diatomic molecular species containing these elements, were readily identified in the emission spectra, providing higher sensitivity than the atomic lines. In the particular case of chlorine, a tenfold improvement on the limit of detection was obtained by Haisch et al., considering the CuCl D-system between 421.10 and 451.59 nm instead of the 837.6 nm Cl emission line [9]. In addition, the alkali earth elements (e.g. Ca and Ba) were shown to easily combine with halogens in the plasma, producing intense emission molecular spectra [10]. Molecular emission bands of CaF were used by Álvarez-Llamas et al. [11] for quantification of fluorine traces in solid samples, achieving a limit

\* Corresponding author.

Email address: bordel@uniovi.es (N. Bordel)

<sup>1</sup> Currently affiliated to the School of Mathematical & Physical Sciences, University of Sussex, Falmer BN19QH, UK.

of detection of  $50 \mu\text{g/g}$ , which is an improvement of one order of magnitude with respect to F atomic-emission-based methods. This approach, first studied for samples containing Ca, is also feasible when Ca is not present intrinsically in the sample but nebulized above its surface [12]. Detection limits using this strategy were reported to be  $49 \mu\text{g/g}$ , matching those obtained in analogous Ca-containing samples. Said research was mainly focused on sensitivity improvements, but the interaction of the nebulization aerosol with the plasma was not investigated.

Therefore, in the present work, the effect of nebulization on the ablation process and on the plasma properties has been thoroughly investigated. In particular, spatio-temporal evolution of a laser induced plasma under different nebulization conditions was evaluated using a high-purity copper standard as model sample, in order to use the same matrix element as in the aforementioned studies [11,12]. Non-containing F samples were considered to avoid the effect of the CaF molecule formation in the plasma, allowing for a more general study of the interaction between the laser induced plasma (LIP) and the nebulized solution. Moreover, parameters such as the emission decay curve of selected Cu I and Cu II lines, and excitation temperatures (obtained using the Boltzmann plot method and assuming local thermodynamic equilibrium (LTE) conditions) were determined.

## 2. Experimental

### 2.1. LIBS set-up

The LIBS experimental set-up used in this work (see Fig. 1) relies on the use of a nanosecond Q-switched Nd:YAG laser (EKSPILA model NL301HT) with a pulse duration of 3–6 ns, operating at 1064 nm and 100 mJ per pulse, set using an attenuator (Lotis Tii). The maximum laser repetition rate is 10 Hz, but it was lowered to match the ICCD reading times. The laser beam has a diameter of approximately 6 mm and is focused into the sample via an objective (Thorlabs, LMH-5 $\times$ -1064) of 35 mm nominal focal length, situated at 33 mm from the sample surface. Light collection can be carried out in two different ways. The first one, corresponding to the set-up used in previous works [11,12], uses two plane-convex lenses (Newport, SPX022AR.10 and Thorlabs, LA4148 with nominal focal lengths 100 and 50 mm, respectively), which focus the light into an optical fiber (Andor, SR-OPT-8014) with its end attached to one of the entrance slits of a spectrograph (Andor Shamrock SR-500i-D1, 500 mm focal length and f/6.5).

A second detection system has been added to the experimental set-up in this work to obtain spatially resolved information of the plasma. It consists of two 2" plane-convex lenses with nominal 150 and 300 mm focal lengths (Thorlabs, LA4904-UV and LA4855-UV, respectively). These lenses provide a 2:1 magnification with a numerical aperture of f/5.94 and collimate and focus the light from the plasma onto the entrance slit plane of the spectrometer. This spectrometer includes a 2400 lines/mm grating as well as a mirror. A  $1024 \times 1024$  pixels ICCD (Andor iStar DH734-25f-03) is attached to the exit of the spectrometer allowing for spatial and time-resolved measurements. The use of the 2400 grooves/mm grating with this ICCD allowed for spectral windows of approximately 15 nm. Calibrated Deuterium (Newport) and Tungsten (Bentham Instruments Limited) lamps were used to obtain the wavelength efficiency curve of the experimental set-up so that emission line intensities were appropriately corrected for accurate excitation temperature calculations.

### 2.2. Time-resolved measurements

Preliminary studies were carried out with the first collection system (see element 4 in Fig. 1). In this case, spectra were obtained applying *full-vertical binning* (FVB) of the ICCD rows, meaning a single spectrum (corresponding to average plasma emission) is obtained in one measurement.

Table 1 summarizes temporal acquisition parameters for the spatially-averaged time-resolved study of the emission. Moreover, delay times between 1 and  $10 \mu\text{s}$  with a constant gate time of  $1 \mu\text{s}$  were employed in the study of the excitation temperature.

### 2.3. Time and space-resolved measurements

The second collection system (see element 5 in Fig. 1) was used for two different acquisition schemes. On the one hand, spatially resolved spectra along the plasma axis were obtained with a slit width of  $100 \mu\text{m}$  at the entrance of the spectrograph. In other experiments, this entrance slit was removed, and the mirror of the spectrograph was used instead of the grating, in order to obtain full images of total emission of the laser-induced plasmas in single measurements. A USAF 1951 resolution target (Thorlabs) was used to determine the spatial resolution of the system, which was set in  $40 \mu\text{m}$  taking into consideration the smallest element (3–6) of the target that was resolved by

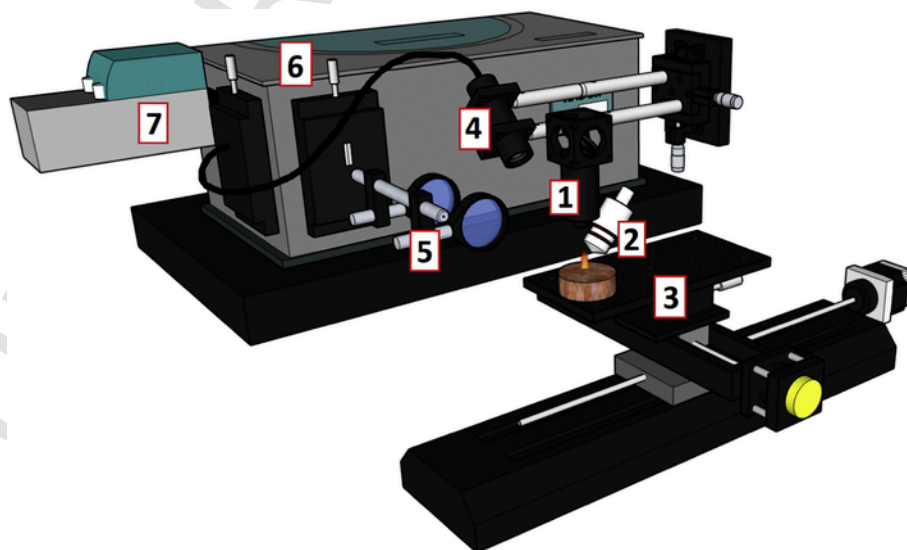


Fig. 1. Depiction of the main elements in the set-up: (1) Focusing objective (2) Total consumption nebulizer (3) Motorized XY and manual Z translation stages (4) Collection lenses for optical fiber measurements (5) Collection lenses for the light focusing onto the entrance slit (6) Czerny-Turner spectrometer with two entrance ports (7) ICCD

**Table 1**  
Experimental conditions for emission evolution studies.

Emission line	Delay range (ns)	Gate time (ns)
Cu II at 254.48 nm	75–5000	50
Cu I at 515.32 nm and 521.82 nm	550–15,000	

our system. Full-image studies were done with a scale of  $10.0 \pm 0.3 \mu\text{m}$ /pixel, determined by measuring the known-sized elements of the resolution target with our system. However, when obtaining spectral information along the vertical axis of the plasma, a binding of 10 ICCD rows ( $100 \mu\text{m}$ ) was done to obtain enough signal and, therefore, in this case spatial resolution corresponds to  $100 \mu\text{m}/\text{group}$ .

The temporal windows considered in the spatially resolved studies are summarized in Table 2. Moreover, temperature profiles were obtained for a delay time of  $5 \mu\text{s}$  and a gate time of  $0.5 \mu\text{s}$ .

#### 2.4. Sample and nebulization experiments

The nebulization scheme was described in a previous work [12] and involves the use of a microflow concentric nebulizer (Teledyne CETAC Technologies) that is directed onto the surface of the solid sample over the laser spot. The nebulized solution, a 1:1 mixture of a 30% w/w calcium nitrite solution (Sigma Aldrich) and ultrapure water, was introduced using a syringe pump (78-9100I, Thermo Fisher Scientific) at a rate of  $0.24 \text{ mL/h}$  using Ar as gas carrier, with a flow rate set to  $0.7 \text{ L/min}$  by a mass flow controller (MKS Instruments). The solid sample used in all of these experiments was a Cu matrix (99.997%) certified reference material from MBH (reference  $9 \times 3-27,869$ ). The emission lines from Cu I and Cu II employed in this work, together with their most relevant spectroscopic characteristics, are listed in Table 3.

### 3. Results and discussion

#### 3.1. Time-resolved study of the plasma emission

First experiments were addressed to explore possible differences in the plasma characteristics when generated under no-nebulization and Ca-solution nebulization conditions. Non-spatially resolved studies were initially considered to investigate laser induced plasma characteristics at these operating conditions. In particular, temporal evolution of the emission and the excitation temperatures were evaluated. These experiments were done using the first collection system and a Cu matrix target as model sample.

The temporal evolutions of two Cu I (515.32 and 521.82 nm) and one Cu II (254.48 nm) emission lines, both under no-nebulization and nebulization conditions, were studied at the delay and gate times indicated in Table 1 for atomic and ionic lines, respectively. Each spectrum was obtained accumulating the plasma emission of 30 laser shots. Fig. 2(a-c) shows the areas under the emission line profiles, after background subtraction and normalization to the maximum signal, versus the acquisition delay time. Each value corresponds to an averaging of 3 replicates, indicating the standard deviation by means of error bars.

**Table 2**  
Temporal windows for total-emission spatially resolved measurements.

Temporal window	Delay ( $\mu\text{s}$ )	Gate time ( $\mu\text{s}$ )
1	0.100	0.003
2	0.50	0.05
3	1.0	0.1
4	5	1
5	9	1
6	30	2

**Table 3**  
Spectroscopic data of the studied Cu lines [13].

Species	$\lambda$ (nm)	$A_{ji}$ ( $\times 10^7 \text{ s}^{-1}$ )	$E_i$ (eV)	$E_j$ (eV)	$J_j$	Study label
Cu II	254.48	19.4	8.522	13.392	3	(1)
Cu I	261.84	3.07	1.389	6.123	3/2	(2)
	276.62	0.960	1.642	6.123	3/2	(2)
	282.44	0.780	1.389	5.777	5/2	(2)
	296.12	0.376	1.389	5.575	7/2	(2)
	402.26	1.90	3.786	6.867	3/2	(2)
	406.26	2.10	3.817	6.868	5/2	(2)
	453.08	8.40	3.817	6.552	1/2	(2)
	453.97	2.12	5.153	7.883	3/2	(2), (3)
	458.70 <sup>a</sup>	3.20	5.102	7.805	5/2	(2), (3)
	465.11	3.8	5.072	7.737	7/2	(2), (3)
	510.55	0.20	1.389	3.817	3/2	(2), (3)
	515.32	6.0	3.786	6.191	3/2	(1), (2), (3)
	521.82	7.5	3.817	6.192	5/2	(1), (2), (3)
	578.21	0.165	1.642	3.786	1/2	(2), (3)

The selected emission lines are employed along this manuscript for different calculations, labeled as: (1) Lines used for temporal evolution of intensity under no nebulization and Ca-solution nebulization, (2) Lines used for temporal evolution of excitation temperature under aforementioned conditions, (3) Lines used for spatially-resolved excitation temperatures study under no nebulization, Ar-flow, ultrapure water nebulization and Ca-solution nebulization.

<sup>a</sup> Not seen with Ca-solution nebulization.

An exponential decay was observed in all the cases. Each decay curve was then fitted to the function  $I = I_0 + A.e^{-\frac{t}{\tau}}$ , where the  $\tau$  parameter provides the time for the signals to decay to a value of 36.8% of the initial one. Fig. 2d. shows the  $\tau$  values calculated for each emission line, with and without solution nebulization of the sample. It is noticed that decay times of Cu ionic and neutral lines are affected by the Ca-containing solution nebulization: the decay time of Cu II line is longer under Ca-solution nebulization ( $448 \pm 10 \text{ ns}$  as opposed to  $320 \pm 11 \text{ ns}$ , a  $\times 1.4$  increase), whereas both Cu I lines decay faster going from  $4.0 \pm 0.2 \mu\text{s}$  and  $3.6 \pm 0.2 \mu\text{s}$  (lines at 515.32 nm and at 521.82 nm, respectively) to  $2.4 \pm 0.2 \mu\text{s}$  and  $2.5 \pm 0.2 \mu\text{s}$ , which are approximately a 65% of the non-nebulized corresponding values. De-excitation processes in the laser induced plasma are clearly affected by the Ca-solution nebulization process.

Fourteen Cu I emission lines (labeled as (2) in the last column of Table 3) with known transition probabilities were used to study the evolution of excitation temperatures in the plasma under non-nebulized and nebulization conditions. Boltzmann plots were obtained at each delay time from 3 to  $10 \mu\text{s}$  with a gate time and delay time steps of  $1 \mu\text{s}$ , discarding lower delay times due to substantial uncertainties in the temperature determination. As an example, Fig. S1(a,b) (Supplementary Information) shows the Boltzmann plots at  $5 \mu\text{s}$  of delay, corresponding to the cases of non-nebulized and nebulized LIP, respectively. The excitation temperatures estimated from the slopes of these graphs,  $9446 \pm 559$  and  $8084 \pm 520 \text{ K}$ , show a decrease of about 14% in the temperature when nebulization is taking place. Fig. 3 shows the temporal evolutions of the calculated excitation temperatures for both cases under study. It is observed that the temperatures decrease at increasing delay times at a similar rate in both cases; however, the temperatures were significantly lower when nebulization was carried out.

#### 3.2. Spatially resolved studies

The previous studies showed noticeable changes in the plasma properties due to the nebulization but provided only spatially-average information of the plasma. To get further insight into plasma modifications under nebulization conditions, experiments with spatial and temporal resolution were carried out. Emission from the plasma was then collected with the second collection system and four situations were studied in order to recognise the individual effect of each component introduced through the nebulization set up. Firstly, measure-

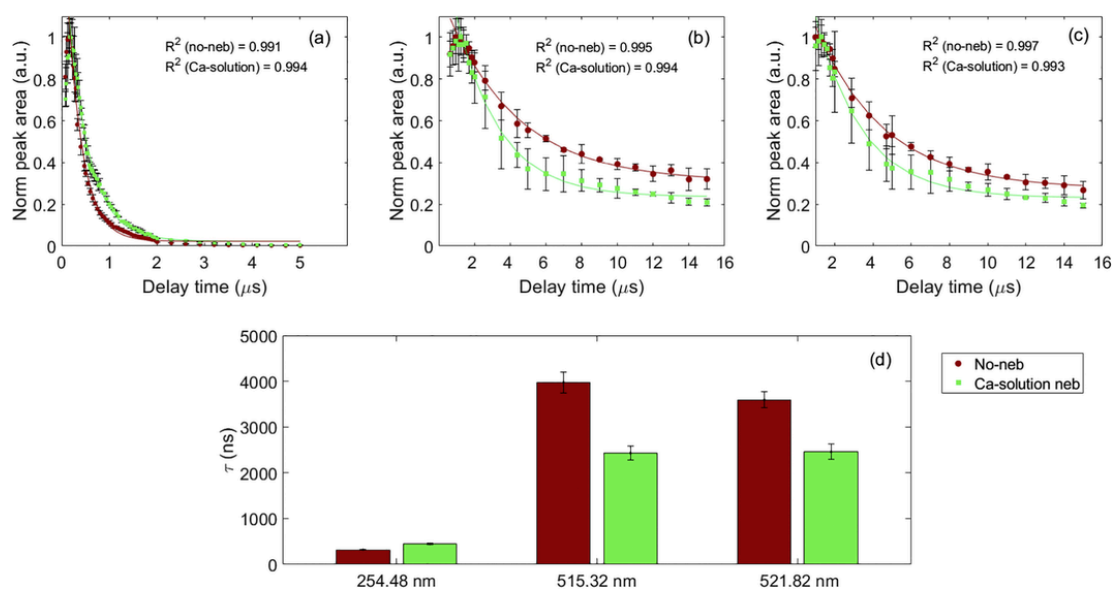


Fig. 2. Evolution of line intensity as a function of delay time for (a) Cu II at 254.48 nm (b) Cu I at 515.32 nm (c) Cu I at 521.82 nm and (d) Decay times of each line under no-nebulization and Ca-solution nebulization.

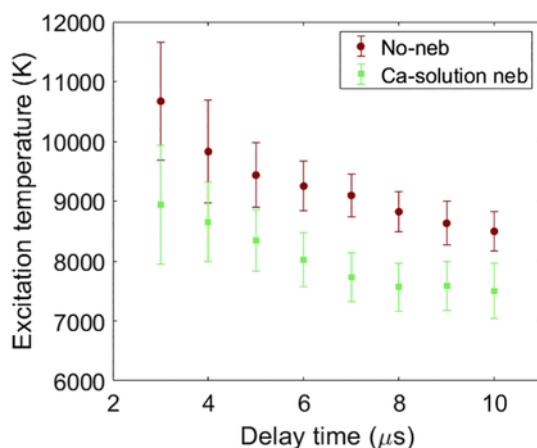


Fig. 3. Evolution of excitation temperature under no-nebulization and Ca-solution nebulization

ments without nebulization were carried out as reference. Then, experiments with the nebulizer supplying: a) only the carrier Ar gas flow, b) carrier gas with ultrapure water nebulization and, c) carrier gas with Ca-containing solution nebulization, were performed and evaluated.

### 3.2.1. Bidimensional characterization of the plasma plumes

Full images of the total plasma emission under the four nebulization conditions previously indicated were collected at 6 different delay times (Table 2) to characterize possible alterations in the plume shape caused by the nebulized aerosol. This study was carried out using the spectrometer in image configuration (without entrance slit and using the mirror instead of the grating to direct the no-diffracted emission light to the detector). The images were obtained as the average of three measurements and, in addition, a gaussian smoothing was used to reduce noise. The 24 images (6 time windows  $\times$  4 experimental conditions) are shown in Fig. S2 (Supplementary information). For an easy visualization of differences of emission under nebulization conditions compared to the non-nebulized case, images in Fig. S2 are normalized to the non-nebulized case at the same time window, and values above 1 are considered as “saturated”. As can be seen noticeable changes in the plasma shape and in its emission intensity, arise when the nebuliza-

tion is taking place. In the next paragraphs the observed changes are analyzed and discussed.

Intensity profiles along the plasma height were obtained averaging a 100  $\mu\text{m}$  region around the central axis in each image. Fig. 4 shows the resulting intensity profiles along the axis of the laser beam for the six different temporal windows investigated and for all four nebulization situations. Non-significant changes were produced by the Argon flow (Fig. 4b), maintaining similar intensities and profiles as the non-nebulized plasma. This could be due to the small amount of Ar being introduced in the plasma region by the nebulizer, which is likely to be significantly diluted in the atmosphere. However, several modifications occur when the ultrapure water is nebulized (Fig. 4c): higher emission intensities are observed, and the maximum intensity region is measured at higher distance to the sample, with respect to previous cases, going from less than 1 mm to 1.5 mm in the fourth temporal window (5–6  $\mu\text{s}$ ). Additionally, the variability of the intensity is higher with water nebulization, as shown by means of the shaded regions, having up to 10% uncertainty ( $N = 3$ ), while non-nebulized and Ar flow cases are under 5%.

Once the Ca-solution was used instead of ultrapure water, full-plasma images revealed major differences in the shape of the plasma with a loss of the axial symmetry during its temporal evolution (Fig. S2). It can be noted in Fig. 4d that the variability of the plasma emission is then at its highest value, with  $> 10\%$  variations in intensity.

Due to the loss of symmetry in the expansion, the profiles in Fig. 4d do not provide a complete picture of the extent of the Ca-solution nebulization's effects on the plasma. Nevertheless, these profiles show remarkable differences compared to the other cases, such as a faster expansion of the plasma plume as seen in the second temporal window or the extended and quite flat emission region in the temporal interval 5–6  $\mu\text{s}$ . In Fig. 5, a more detailed plasma evolution for the Ca-solution nebulization case is shown. Some relevant aspects can be pointed out. As expected, a semispherical expansion of the plume was observed at delays of less than 1  $\mu\text{s}$ . Afterwards, the plasma growth took place mostly along the laser's incidence axis, until the upper region was detached from the main plume at approximately 9  $\mu\text{s}$  of delay. Then, a highly unstable-shaped plasma was noticed in the lower region.

This detached emitting region appeared slightly tilted towards the nebulizer, which was approximately set at 50 degrees with respect to the sample's surface (see Fig. 1). The underlying mechanism be-

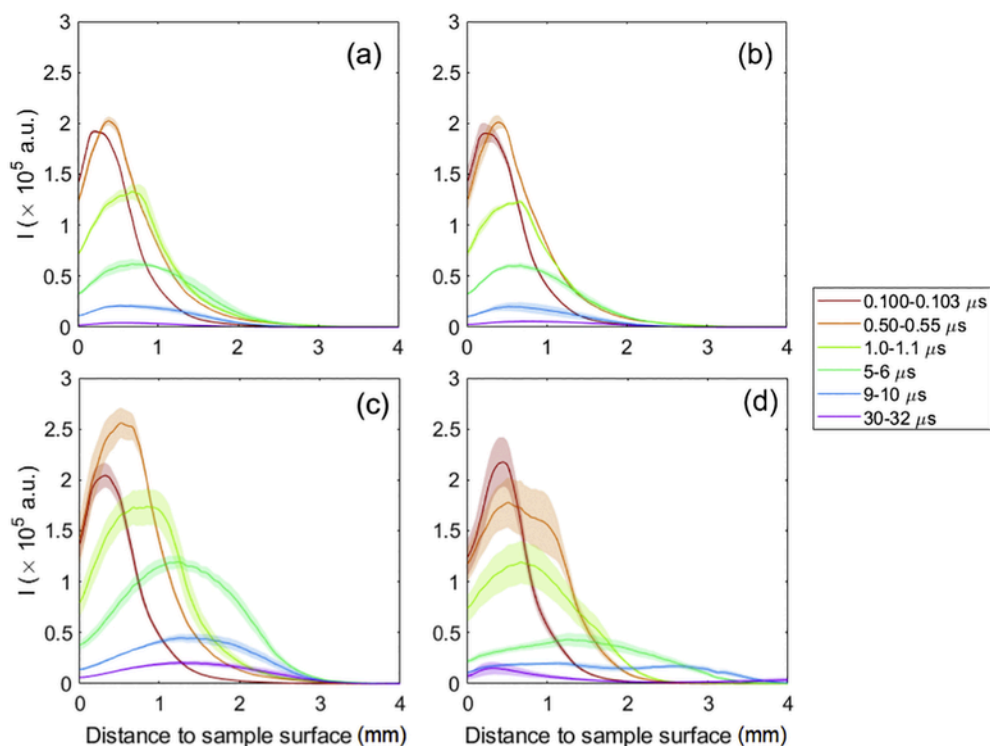


Fig. 4. Intensity profiles along the laser incidence axis with (a) no nebulization (b) carrier gas flow (c) ultrapure water nebulization (d) Ca-solution nebulization for different temporal windows.

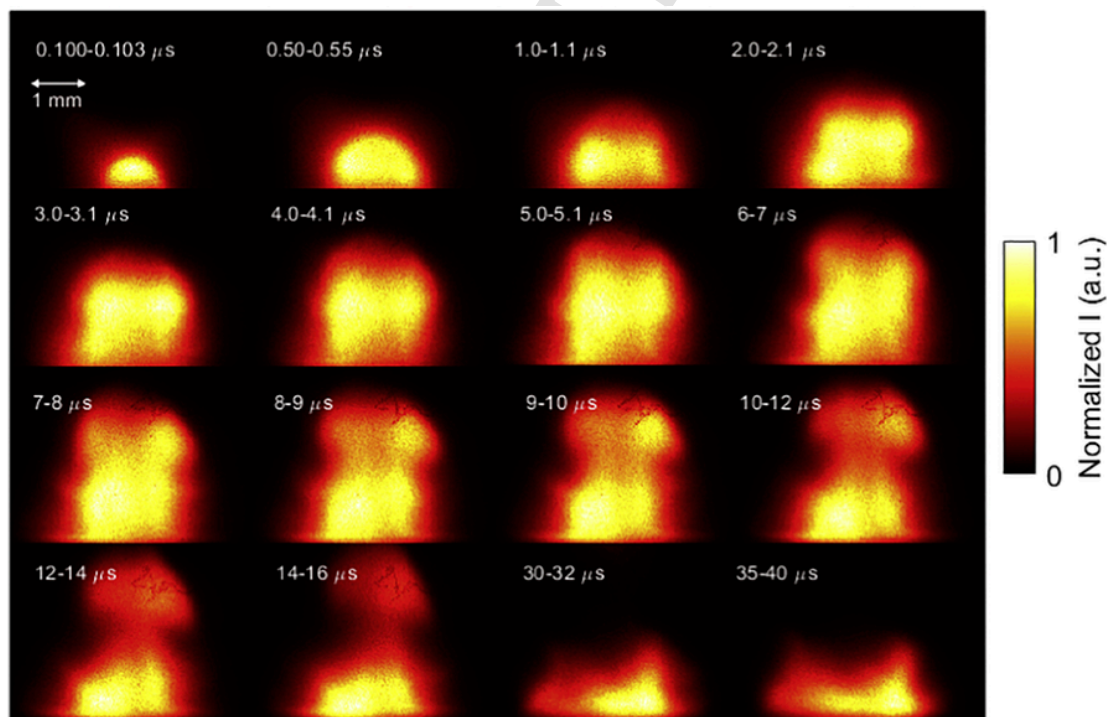


Fig. 5. Complete evolution of the Ca-solution nebulized plasma normalized emission.

hind this phenomenon is unclear; plasma-aerosol interaction could be causing the dissociation and vaporization of the aerosol particles [14], and the aerosol presence could be creating a favorable region for the plasma expansion. In any case, since this process is not observed with the ultrapure water nebulized aerosol, it is clear that the Ca-solution plays an important role, with its nebulization affecting the experimen-

tal conditions in a different and more remarkable manner than ultrapure water alone.

The intensity distribution of the plasma plume differed from all other cases; instead of showing the highest intensity at its central axis, two bright lobules with a lower intensity area in between were observed. The most intense region was in the opposite side to the nebu-

lizer during most of the temporal evolution with the exception of the last two time windows (30–32 μs and 35–40 μs in Fig. 5).

Given that plasma shapes, when Ca-solution is nebulized, strongly differ from the other cases, the respective maximum intensities of the plasmas at each temporal window were compared (Fig. 6a). To properly interpret these graphs, it must be remarked that each temporal window has a different duration. Therefore, this figure is mainly considered to compare the emission under different nebulization conditions at the same temporal window. The dotted line connecting the points in each case is just for ease of the comparison. It can be observed that only ultrapure water nebulization was found to produce a significant increase in maximum intensity at all temporal windows. Additionally, to compare the whole emission at each temporal window for the four experimental conditions, the total intensity for each image, which consists on a 4 × 5 mm rectangle where the base corresponds to the sample surface, was calculated and plotted (Fig. 6b). This comparison shows that two differentiated behaviors take place: non-nebulized and Ar-flow cases display almost identical integrated intensities, while both ultrapure water and Ca-solution nebulization produce a remarkable increment. The early stages of the plasma plume expansion under ultrapure water and Ca-solution nebulization show the same integrated intensity values, but the integrated emission for the ultrapure water nebulization case remains with high values for longer time.

### 3.2.2. Excitation temperatures along the laser incidence axis

Excitation temperature profiles along the central vertical axis of the plasma were obtained for a given temporal window (5.0 to 5.5 μs) to further characterize the effects of the nebulization process. The atomic emission lines utilized to obtain the Boltzmann plots, which in-

volve high, medium and low upper energy levels of Cu, are listed in Table 3 (labeled as (3) in the last column). Four different spectral windows were used to acquire the signal intensities of the emission lines selected, since the 2400 grooves/mm diffraction grating only allowed a range of 15 nm per spectral window.

Fig. 7 shows the emission spectra measured in the 510–525 nm region, at the selected time window, at different distances to the sample surface, with and without nebulization. It is observed that despite having the same order of magnitude of total-intensity, along the axis (see Fig. 4a and d), copper emission lines are actually one order less intense when the Ca-solution is nebulized. This is in agreement with previous studies on the effect of the presence of calcium on the emission signal of other elements in ICP-AES [15], which showed a significant decrease attributed to the plasma energy required for the dissociation of the nebulized substance. In addition, Cu emission lines exhibit completely different spatial distribution, the maximum Cu emission line intensities are closer to the sample in the non-nebulized case compared to the Ca-solution nebulization case, which is in agreement with results for the distribution of the total light along the axis showed in Fig. 4.

Once the intensities of the seven selected Cu emission lines at different distances to the sample were measured for the four experimental conditions, the Boltzmann plots were obtained using the spectroscopic data collected in Table 3. As an example Fig. S3 (Supplementary information) shows the Boltzmann plots determined at a distance of 1.0–1.1 mm to the sample surface being the estimated excitation temperatures around 12,000 K for all the cases, except for the Ca-solution nebulization case where a temperature of about 8000 K was obtained. The excitation temperatures were calculated up to a distance-to-sample where the Boltzmann plots were still linear (taking  $R^2 > 0.8$  as crite-

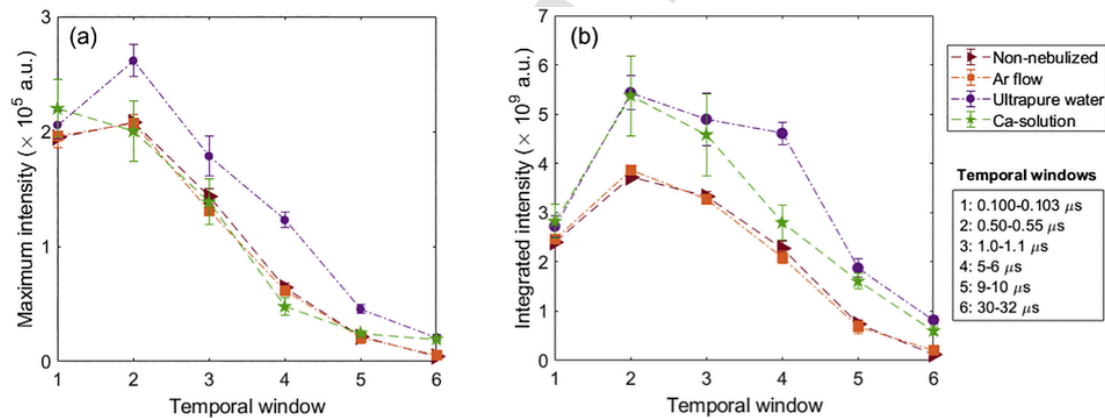


Fig. 6. (a) Maximum total-light intensities at each time and condition. (b) Integrated image intensity in each 4 × 5 mm frame. Temporal windows according to Table 2.

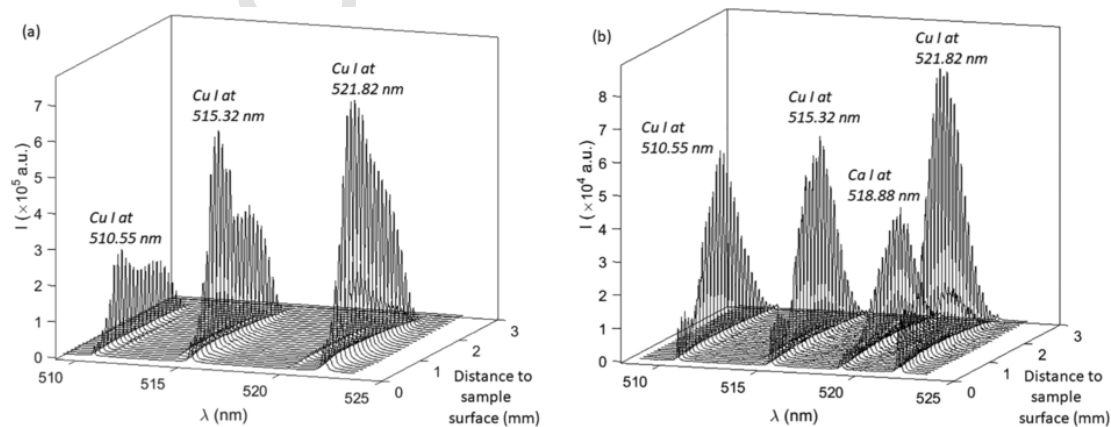


Fig. 7. Comparison of (a) non-nebulized and (b) Ca-solution nebulized plasmas line intensities in the 510–525 nm region.

ria), and where no data point showed a remarkable increment in its uncertainty due to a very low intensity of the corresponding emission line.

Fig. 8 shows the excitation temperature profiles obtained for the four nebulization cases under study, displaying the corresponding uncertainties by means of shaded regions. In addition, inset figures show the R-squares from the Boltzmann plots calculated at different distances to the sample surface. For all cases, except for ultrapure water nebulization, the points at the Boltzmann plots were accurately distributed in a linear trend, with R-squares over 0.98 for most of the profiles. It is remarked that lower Cu excitation temperature were obtained under Ca-solution nebulization conditions (8000 K versus 12,000 K), which agrees with non-spatially resolved results shown in Fig. 3. Inversely, water nebulization is observed to produce a small increment of the temperature excitation with respect to the non-nebulized and Ar-flow conditions, although excitation temperature uncertainties were more pronounced. It has to be noted that lower plasma excitation temperatures when a Ca-solution nebulization is employed instead of other solution or water nebulization, was also observed in ICP-AES studies [16,17].

### 3.3. Crater characterization

During the experiments, it was observed that nebulization had a remarkable effect on the laser-induced crater appearance. Therefore, crater profiles were measured using a profilometer (Mahr PERTHERN Perthometer S5P) and a representative example is plotted in Fig. 9. Each crater is the result of 240 shots (10Hz, 100mJ). A noticeable re-deposition was observed in the non-nebulized and Ar-flow cases, but it was less significant for the other nebulization conditions. In the case of the Ca-solution nebulization, the craters were remarkably smooth and deeper than in any other case. Moreover, the surface of the sample was observed to show blue-colored regions after Ca-solution nebulization. This could be due to a chemical reaction of nitric acid and copper and might be taking part in the crater smoothing. Considering also the ul-

trapure water case, the ablation rate also appeared to be increased by the nebulization of a liquid. The increment in ablation rate (up to a  $3 \times$  factor) could be attributed to a lens effect of the water aerosol droplets, already reported by Cabalín et al. [18]. It is worth noting that the presence of the continuous aerosol could affect the transmission of the laser beam towards the sample since absorption or scattering by the aerosol particles could take place. However, the increase of ablation due to the aforementioned lens effect could be compensating for a possible energy decrease reaching the Cu target.

The increment in the ablation rate when ultrapure water is nebulized could explain the increase of the integrated image intensity observed in Fig. 6b since a noteworthy enhance of the Cu emission lines under ultrapure nebulization, compared to the case of no-nebulization, was confirmed from the study of the spectra used to obtain the excitation temperature. Nevertheless, it should be remarked that, in spite of the higher ablation rate of the Cu matrix sample, the nebulization of Ca-solutions produced a decrease of about one order of magnitude in the evaluated Cu emission lines (Fig. 7). In consequence the higher integrated image intensity obtained (Fig. 6b) should be due to the contribution of other excited species, incorporated in the plasma by the nebulization of the Ca-solution.

## 4. Conclusions

Laser-induced plasma under different nebulization conditions were investigated. A high-purity copper standard was used as model sample. The temporal evolution of Cu ionic and neutral emission lines was studied under no nebulization and under Ca-solution nebulization, showing a significant modification of their intensity decay. In particular, the nebulization of Ca-solution produced a slower decrease of the emission intensity for the ionic line (45% increase of the decay parameter), and the opposite effect on the neutral lines. Additionally, Ca-solution nebulization produced lower average Cu excitation temperatures independently of the temporal window investigated.

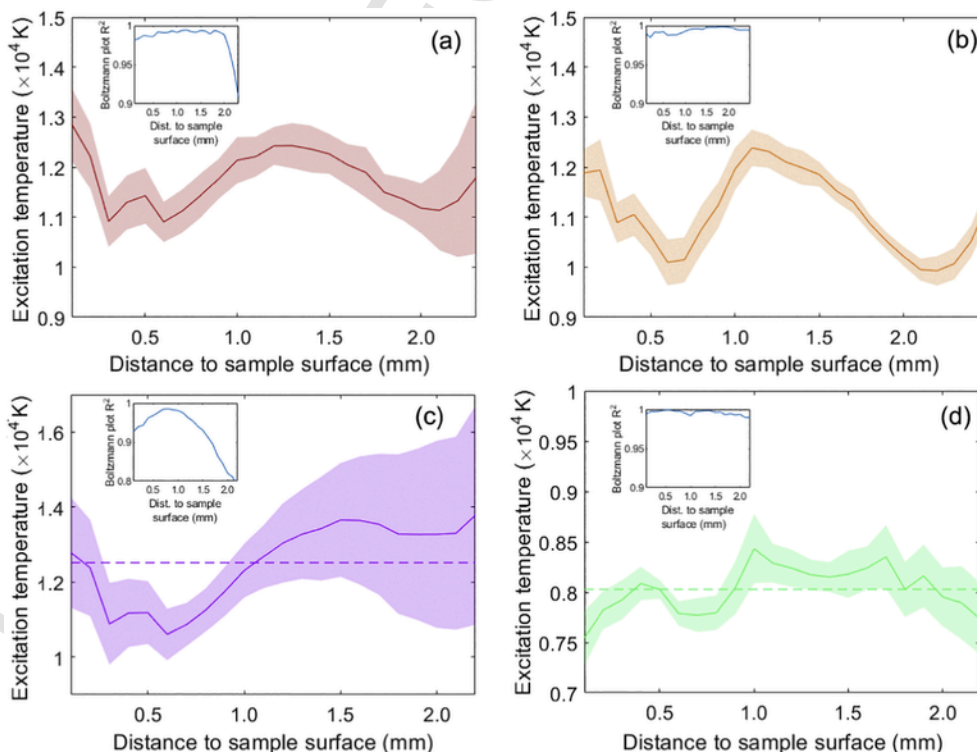


Fig. 8. Excitation temperature profiles obtained in (a) Non-nebulized (b) Ar-flow (c) Ultrapure water nebulization and (d) Ca-solution nebulization cases

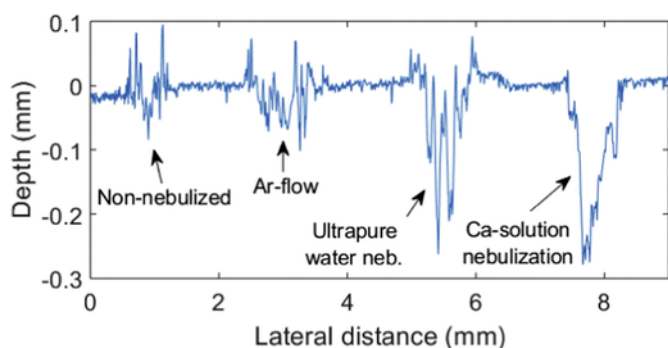


Fig. 9. Depth profiles of craters under each of the studied conditions.

A more detailed study including spatial resolution and considering the different components present in the nebulization scheme showed that Ar-flow under the evaluated experimental conditions was not sufficient to modify either the plasma plume shape, the total emission intensities or the crater compared to the non-nebulized case. Ultrapure water nebulization increases sample ablation, and the plasma plume size. In addition, the maximum intensity as well as the integrated image intensity are higher than the ones obtained with no-nebulization, at each temporal window; however, there is non-significant change in the Cu excitation temperature. The Ca-solution nebulization provided an increment of the ablation rate in the Cu target (similar to that observed when ultrapure water is nebulized), but in this case, unlike the ultrapure water nebulization case, the intensities of the Cu emission lines under study were one order of magnitude lower than those measured with no-nebulization. Nevertheless, the integrated image intensity, took values similar to those measured when ultrapure water was nebulized. These results show that the presence of Ca-solution droplets in the plasma strongly affect the Cu excitation, reducing its emission in spite of the higher amount of Cu atoms present in the media. Overall plasma emission is higher than in the non-nebulized case due to other species, mainly Ca, that are contributing to the total intensity.

The shape of the plasma plume was heavily influenced by the Ca-solution nebulization, displaying a huge asymmetry and a detachment of the upper region at around 9  $\mu$ s of delay. Both characteristics were absent in other cases. The spatially resolved excitation temperatures profiles also showed lower values under Ca solution nebulization.

This is a preliminary study where the effect of the nebulization is examined in a pure copper plasma. Having observed that remarkable differences are indeed produced, it is of interest to further characterize the effect of the nebulization in a F-containing plasma where molecule species (CaF) will be formed due to recombination processes. Moreover, additional diagnostic parameters such as the electronic densities, are needed to further characterize the laser-induced plasma.

CRediT authorship contribution statement

**C. Méndez-López:** Conceptualization, Investigation, Writing - original draft, Writing - review & editing. **R. Álvarez-García:** Conceptualization, Investigation. **C. Álvarez-Llamas:** Conceptualization, Investigation, Writing - review & editing. **L.J. Fernández-Menéndez:** Conceptualization, Investigation. **C. González-Gago:** Writing - review & editing, Supervision. **J. Pisonero:** Conceptualization, Funding acquisition, Writing - review & editing, Supervision. **N. Bordel:** Conceptualization, Investigation, Funding acquisition, Writing - review & editing, Supervision.

## Declaration of Competing Interest

The authors declare no conflict of interest.

## Acknowledgements

The authors would like to gratefully acknowledge the financial support from the Government of the Principality of Asturias and the European Regional Development Fund through the project FC-GRUPIN-IDI/2018/000186 and from the Spanish Government through the project MINECO 17-CTQ2016-77887-C2-1R.

## Appendix A. Supplementary data

Supplementary data to this article can be found online at <https://doi.org/10.1016/j.sab.2020.105906>.

## References

- [1] P. Lucena, A. Doña, L. Tobaría, J. Laserna, New challenges and insights in the detection and spectral identification of organic explosives by laser induced breakdown spectroscopy, *Spectrochim. Acta - Part B At. Spectrosc.* 66 (2011) 12–20.
- [2] C. López-Moreno, S. Palanco, J. Laserna, F.D. Lucia, A. Miziolek, J. Rose, et al., Test of a stand-off laser-induced breakdown spectroscopy sensor for the detection of explosive residues on solid surfaces, *J. Anal. At. Spectrom.* 21 (2006) 55–60.
- [3] Á. Fernández-Bravo, P. Lucena, J. Laserna, Selective sampling and laser-induced breakdown spectroscopy (LIBS) analysis of organic explosive residues on polymer surfaces, *Appl. Spectrosc.* 66 (2012) 1197–1203.
- [4] M. Baudelet, L. Guyon, J. Yu, J. Wolf, T. Amodeo, E. Frejafon, et al., Spectral signature of native CN bonds for bacterium detection and identification using femtosecond laser-induced breakdown spectroscopy, *Appl. Phys. Lett.* 88 (2006) 3–5.
- [5] A. Boyain-Goitia, D. Beddows, B. Griffiths, H. Telle, Single-pollen analysis by laser-induced breakdown spectroscopy and Raman microscopy, *Appl. Opt.* 42 (2003) 6119–6132.
- [6] F. Doucet, P. Faustino, M. Sabsabi, R. Lyon, Quantitative molecular analysis with molecular bands emission using laser-induced breakdown spectroscopy and chemometrics, *J. Anal. At. Spectrom.* 23 (2008) 694–701.
- [7] H. Niki, T. Yasuda, K. Iwao, Measurement technique of boron isotopic ratio by laser-induced breakdown spectroscopy, *J. Nucl. Sci. Technol.* 35 (1998) 37–41.
- [8] A. Bolshakov, X. Mao, J. Gonzalez, R. Russo, Laser ablation molecular isotopic spectrometry (LAMIS): current state of the art, *J. Anal. At. Spectrom.* 31 (2014) 119–134.
- [9] C. Haisch, R. Niessner, O. Matveev, U. Panne, N. Omenetto, Element-specific determination of chlorine in gases by laser-induced-breakdown-spectroscopy (LIBS), *Fresenius J. Anal. Chem.* 356 (1996) 21–26.
- [10] M. Gaft, L. Nagli, N. Eliezer, Y. Groisman, O. Forni, Elemental analysis of halogens using molecular emission by laser-induced breakdown spectroscopy in air, *Spectrochim. Acta - Part B At. Spectrosc.* 98 (2014) 39–47.
- [11] C. Álvarez-Llamas, J. Pisonero, N. Bordel, Quantification of fluorine traces in solid samples using CaF molecular emission bands in atmospheric air laser-induced breakdown spectroscopy, *Spectrochim. Acta - Part B At. Spectrosc.* 123 (2016) 157–162.
- [12] C. Álvarez-Llamas, J. Pisonero, N. Bordel, A novel approach for quantitative LIBS fluorine analysis using CaF emission in calcium-free samples, *J. Anal. At. Spectrom.* 32 (2017) 162–166.
- [13] A. Kramida, Y. Ralchenko, J. Reader, NIST ASD Team, National Institute of Standards and Technology, Gaithersburg, MD, [Online]. Available <https://physics.nist.gov/asd>, 2019.
- [14] M.E. Asgill, D.W. Hahn, Particle size limits for quantitative aerosol analysis using laser-induced breakdown spectroscopy: temporal considerations, *Spectrochim. Acta - Part B At. Spectrosc.* 64 (10) (2009) 1153–1158.
- [15] I.B. Brenner, A. Zander, M. Cole, A. Wiseman, Comparison of axially and radially viewed inductively coupled plasmas for multi-element analysis: effect of sodium and calcium, *J. Anal. At. Spectrom.* 12 (9) (1997) 897–906.
- [16] B. Budič, Matrix effects in inductively coupled plasma atomic emission spectrometry using an ultrasonic nebulizer, *J. Anal. At. Spectrom.* 13 (9) (1998) 869–874.
- [17] M.H. Ramsey, M. Thompson, A predictive model of plasma matrix effects in inductively coupled plasma atomic emission spectrometry, *J. Anal. At. Spectrom.* 1 (3) (1986) 185–193.
- [18] L. Cabalin, A. Gonzalez, V. Lazic, J. Laserna, Laser-induced breakdown spectroscopy of metals covered by water droplets, *Spectrochim. Acta - Part B At. Spectrosc.* 74-75 (2012) 95–102.